Excitation–contraction coupling is unaffected by drastic alteration of the sequence surrounding residues L720–L764 of the α_{1S} II-III loop

Christina M. Wilkens[†], Nicole Kasielke[‡], Bernhard E. Flucher[‡], Kurt G. Beam[†], and Manfred Grabner[‡§]

[‡]Institut für Biochemische Pharmakologie, Universität Innsbruck, Peter-Mayr-Strasse 1, A-6020 Innsbruck, Austria; and [†]Department of Anatomy and Neurobiology, College of Veterinary Medicine and Biomedical Sciences, Colorado State University, Fort Collins, CO 80523

Edited by Michael J. Berridge, The Babraham Institute, Cambridge, United Kingdom, and approved March 9, 2001 (received for review December 22, 2000)

The II-III loop of the skeletal muscle dihydropyridine receptor (DHPR) α_{1S} subunit is responsible for bidirectional-signaling interactions with the ryanodine receptor (RyR1): transmitting an orthograde, excitation–contraction (EC) coupling signal to RyR1 and receiving a retrograde, current-enhancing signal from RyR1. Previously, several reports argued for the importance of two distinct regions of the skeletal II-III loop (residues R681–L690 and residues L720–Q765, respectively), claiming for each a key function in DHPR–RyR1 communication. To address whether residues 720–765 of the II-III loop are sufficient to enable skeletal-type (Ca^{2+} entry-independent) EC coupling and retrograde interaction with RyR1, we constructed a green fluorescent protein (GFP)-tagged chimera (GFP-SkLM) having rabbit skeletal (Sk) DHPR sequence except for a II-III loop (L) from the DHPR of the house fly, *Musca domestica* (M). The *Musca* II-III loop (75% dissimilarity to α_{1S}) has no similarity to α_{1S} in the regions R681–L690 and L720–Q765. GFP-SkLM expressed in dysgenic myotubes (which lack endogenous α_{1S} subunits) was unable to restore EC coupling and displayed strongly reduced Ca^{2+} current densities despite normal surface expression levels and correct triad targeting (colocalization with RyR1). Introducing rabbit α_{1S} residues L720–L764 into the *Musca* II-III loop of GFP-SkLM (substitution for *Musca* DHPR residues E724–T755) completely restored bidirectional coupling, indicating its dependence on α_{1S} loop residues 720–764 but its independence from other regions of the loop. Thus, 45 α_{1S}-residues embedded in a very dissimilar background are sufficient to restore bidirectional coupling, indicating that these residues may be a site of a protein–protein interaction required for bidirectional coupling.

Excitation–contraction (EC) coupling depends on the interaction of the voltage-gated L type Ca^{2+} channel or dihydropyridine receptor (DHPR) of the plasma membrane and the intracellular Ca^{2+}-release channel or ryanodine receptor (RyR) of the sarcoplasmic reticulum (SR) (reviewed in refs. 1 and 2). Because EC coupling in skeletal muscle still occurs after blocking of the L type Ca^{2+} current, it is thought that membrane depolarization causes conformational changes of the DHPR (3, 4), which, in turn, trigger the opening of the RyR and the release of Ca^{2+} from SR stores ("mechanical hypothesis" of skeletal muscle EC coupling; ref. 3). In addition to this orthograde EC coupling signal, a retrograde signal exists, by which RyR1 (the skeletal isoform of the RyR) enhances L type current through the DHPR (5). Specifically, Ca^{2+} currents are small in dyspedic myotubes (which lack RyR1) despite normal densities of the DHPR, whereas expression of recombinant RyR1 restores the L type current density toward wild-type levels (5).

A fundamental goal for understanding the mechanism of bidirectional signaling is to identify the domains of the skeletal DHPR that directly participate in this process. One approach has been to analyze skeletal/cardiac chimeric DHPRs expressed in dysgenic myotubes, which lack the α_{1S} subunit of the skeletal DHPR (6). Almost 10 years ago, this work demonstrated that a cardiac DHPR containing the skeletal II-III loop was able to restore Ca^{2+} entry-independent (skeletal-type) EC coupling (7). A subsequent study identified 46 aa (residues 720–765) of the skeletal II-III loop that are sufficient for transferring strong, skeletal-type EC coupling properties to an otherwise cardiac DHPR (8). More recently, it was shown that a skeletal DHPR with a cardiac II-III loop (SkLC) lacked both orthograde (skeletal EC-coupling) and retrograde (L current-enhancing) signaling (9). When α_{1S} residues 720–765, which earlier had been shown to confer skeletal-type coupling on an otherwise cardiac DHPR (8), were introduced into SkLC, both skeletal-type EC coupling and wild-type Ca^{2+} current densities were restored (9). Thus, residues 720–765 of the skeletal DHPR II-III loop represent a "critical domain" for the bidirectional interaction between the skeletal DHPR and RyR1.

A limitation of chimeras is that they do not test the functional importance of regions that are conserved between the two parental proteins. This is a significant problem for the cardiac and skeletal DHPRs because the regions flanking the 46-residue critical domain are 56% identical between the cardiac and skeletal II-III loops. The potential importance of these flanking domains is emphasized by the results of experiments testing the effects of peptides on the function of RyR1 *in vitro* (ryanodine binding or Ca^{2+} release in SR vesicular preparations and open probability of RyRs reconstituted in artificial planar bilayers). In the earliest of these studies (10), recombinant peptides corresponding to either the skeletal or cardiac II-III loop were found to activate RyR1, which is difficult to reconcile with the results obtained with the chimeras (see above; refs. 7–9). Later, synthetic peptides (peptide A: α_{1S} residues 671–690; peptide As10: residues 681–690), which corresponded to smaller portions of the skeletal loop and were upstream from the critical domain identified in the chimera studies, were found to activate RyR1 (11–14). In addition to the skeletal peptide (As10), the corresponding cardiac peptide (Ac10), which is homologous because of similar clusters of positively charged residues, also was found to cause activation of RyR1, although to a somewhat lower extent (15). Similar cardiac peptides also have been reported not to cause activation of RyR1 (16). Thus, the significance of the II-III loop-flanking domains remains uncertain.

Although the peptide experiments have the important advantage of providing a test of whether the skeletal DHPR and RyR1 interact directly, they have the disadvantage of lacking physiological context. To test the importance of the regions flanking the critical domain (L720–L764), including the As10 region, we created the chimera SkLM, a skeletal DHPR with a II-III loop from the house fly (*Musca domestica*) DHPR (17), which is highly divergent from both the skeletal and cardiac loops. SkLM

This paper was submitted directly (Track II) to the PNAS office.

Abbreviations: DHPR, dihydropyridine receptor; RyR, ryanodine receptor; EC, excitation–contraction; GFP, green fluorescent protein; SR, sarcoplasmic reticulum; Sk, skeletal.

[§]To whom reprint requests should be addressed. E-mail: manfred.grabner@uibk.ac.at.

The publication costs of this article were defrayed in part by page charge payment. This article must therefore be hereby marked "*advertisement*" in accordance with 18 U.S.C. §1734 solely to indicate this fact.

was unable to support bidirectional coupling, but insertion of α_{1S} residues L720–L764 into the *Musca* loop completely restored both orthograde and retrograde signaling. Thus, residues 720–764 represent or contain the sequence sufficient to mediate bidirectional coupling and, therefore, represent a potential site of protein–protein interaction necessary for this coupling. By contrast, the flanking domains are unlikely to be involved in such protein–protein interactions.

Materials and Methods

Construction of DHPR Chimeras. DHPR II-III loop chimeras were constructed as follows, with nucleotide numbers given in parentheses and asterisks indicating restriction sites introduced by PCR.

Green fluorescent protein (GFP)-α_{1S}. The cDNA coding sequence of the rabbit skeletal muscle DHPR α_{1S} subunit (18) was inserted in-frame 3′ to the coding region of GFP contained in a mammalian expression plasmid, as described previously (19).

GFP-SkLM. The *Eco*RI-*Bal*I fragment of the rabbit skeletal muscle DHPR α_{1S} subunit (*Sk*) (nucleotides 1007–1973) was coligated with the *Bal*I-*Nde*I fragment (nucleotides 1982–2296) from the II-III loop (*L*) from the body-wall muscle DHPR α_1 subunit (*M*) of *M. domestica* (17) into plasmid pSP72 (Promega) by using the internal *Nde*I site (plasmid nucleotide 2379) and the *Eco*RI site of the polylinker. The *Nde*I/*Eco*RI restriction sites of pSP72 also were used to coligate two cDNA fragments, the *Nde*I*-*Xho*I fragment that was PCR-generated from the clone GFP-SkLC, GFP-α_{1S} with the cardiac ($\alpha_{1C,}$ *C*) II-III loop (nucleotides C2716–Sk2654) (9), plus the *Xho*I-*Bgl*II fragment of Sk (nucleotides 2654–4488). The PCR primer used to introduce the *Nde*I* site also mutated 2 aa of α_{1C} (A907, S908) to the corresponding *Musca* residues (G767, T768: see Fig. 1). In a subsequent step, fragments *Eco*RI-*Nde*I (nucleotides Sk1007–M2297) and *Nde*I*-*Bgl*II (nucleotides C2716–Sk4488) were isolated from the two pSP72 subclones and coligated into the *Eco*RI/*Bgl*II-cleaved pSP72 vector. Finally, the *Sal*I-*Eco*RI fragment of Sk (nucleotide 5′ polylinker-1007) was coligated with the *Eco*RI-*Bgl*II fragment (nucleotides Sk1007–Sk4488) from the last pSP72 subclone into the *Sal*I/*Bgl*II sites of plasmid GFP-α_{1S}.

GFP-SkLMS$_{45}$. The *Mfe*I-*Xba*I* fragment of M (nucleotides 2024–2177) was coligated with the *Xba*I*-*Xho*I fragment of GFP-SkLM (nucleotides M2258–Sk2654) into the *Mfe*I/*Xho*I-cleaved plasmid GFP-SkLM. Together with the *Xba*I* (nucleotide M2177) site, the antisense PCR primer introduced an upstream *Afl*II* site (nucleotide M2171). Similarly, the sense primer introduced an additional *Cla*I* site (nucleotide M2265) downstream of the *Xba*I* (nucleotide M2258)-cloning site. To yield plasmid GFP-SkLMS$_{45}$, an *Afl*II*-*Taq*I* fragment of Sk (nucleotides 2159–2292) was ligated into the *Afl*II*/*Cla*I* sites of this subclone. All segments of cDNA generated and modified by PCR were checked by sequence analysis (MWG Biotec, Ebersberg, Germany).

Expression of cDNA. The DHPR cDNAs were expressed in myotubes obtained as primary cultures from newborn dysgenic (*mdg*/*mdg*) mice (20) or myotubes produced by differentiation of the dysgenic cell line GLT (21). GLT cultures were transfected at the onset of myoblast fusion (2–4 days after addition of differentiation medium) by using the liposomal transfection reagent *FuGene* according to the manufacturer's protocol (Roche Diagnostics, Mannheim, Germany). Primary dysgenic myotubes were microinjected into a single nucleus (22) with solutions of DHPR cDNA (100–200 ng/μl) approximately 1 week after initial plating. Two to four days after transfection or injection, expressing myotubes were identified by GFP fluorescence and used in the experiments.

Electrophysiological Characterization. Whole-cell patch clamp (23) recording of Ca^{2+} currents and charge movements (24) was used to obtain an estimate of the ratio of maximum Ca^{2+} conductance to maximum immobilization-resistant charge movement (G_{max}/Q'_{max}), which provides a quantitative assessment of the strength of retrograde coupling. EC coupling was assayed in primary myotubes, as contractions in response to pulses (100 ms, 100 V) applied via an extracellular pipette (22), and in GLT myotubes, as fluorescence transients evoked in cells loaded with Fluo-4AM and stimulated with pulses (1 ms, 20–30 V) applied via electrodes placed on opposite sides of the culture dish (25). To further assess EC coupling, depolarization-induced intracellular Ca^{2+} transients were measured microphotometrically during whole-cell recordings of primary myotubes by including tetrapotassium-Fluo-3 (Molecular Probes) in the pipette solution (26). All electrophysiological procedures, including test protocols, equipment, solutions, and calculations essentially were the same as described recently for primary myotubes (9) or GLT myotubes (25), except that intracellular Ca^{2+} transients were recorded in the present study from primary myotubes expressing fluorescing GFP-tagged chimeras instead of coexpressing the CD8 reporter gene (9).

Immunofluorescence Labeling. Differentiated GLT cultures expressing GFP-SkLM were fixed and immunostained as described previously (27), using an affinity-purified anti-GFP antibody (Molecular Probes) at a dilution of 1:4,000 and the affinity-purified antibody 162 against RyR1 at a dilution of 1:5,000 (28). In double-labeling experiments, Alexa-conjugated secondary antibodies were used for GFP-SkLM so that the antibody label and the intrinsic GFP signal both were recorded in the green channel, and Texas red-conjugated secondary antibodies were used for RyR1. Controls, such as the omission of primary antibodies and incubation with inappropriate antibodies, were routinely performed. Images were recorded on a Zeiss Axiophot microscope by using a cooled charge-coupled device camera and METAVIEW image-processing software (Universal Imaging, Media, PA). At least three different experiments were performed for comparison of the wild-type DHPR (GFP-α_{1S}) with the DHPR chimera GFP-SkLM. Semiquantitative evaluation of the labeling patterns (25) revealed a clustering efficiency of greater than 50% in each experiment.

Results and Discussion

An Ancestral DHPR II-III Loop as a Tool to Test DHPR–RyR1 Interactions. Previous analysis of chimeric DHPRs constructed from skeletal and cardiac sequence showed that a "critical domain" of the α_{1S} II-III loop (residues L720–Q765) is required for both skeletal-type EC coupling (8, 9) and RyR1-mediated enhancement of Ca^{2+} currents (9). However, these experiments provided little or no information about the loop regions that flank the critical domain because these regions are well conserved between the cardiac and skeletal proteins (Fig. 1*B*). In the present work, we tested the importance of these flanking domains by replacing them with highly divergent sequences. To accomplish this, we created the chimera GFP-SkLM (Fig. 1*A*), in which the II-III loop of α_{1S} was replaced by the highly divergent II-III loop of a DHPR cloned from the housefly (*M. domestica*) (17). Although we have not been able to express the *Musca* α_1 subunit functionally in various heterologous systems (*Xenopus* oocytes, tsA-201 cells, or dysgenic myotubes), we did find that constructs containing parts of the *Musca* DHPR sequence were valuable for fine mapping of the DHP-binding domain (29). The *Musca* II-III loop has comparable length (126 residues) to the cardiac and skeletal loops, but only 19% overall identity, most of which is concentrated at the two ends. Importantly, there is absolutely no homology to the peptide A-10 (As10/Ac10) region (Fig. 1*B*); this region has been suggested to be important in EC coupling

PHYSIOLOGY

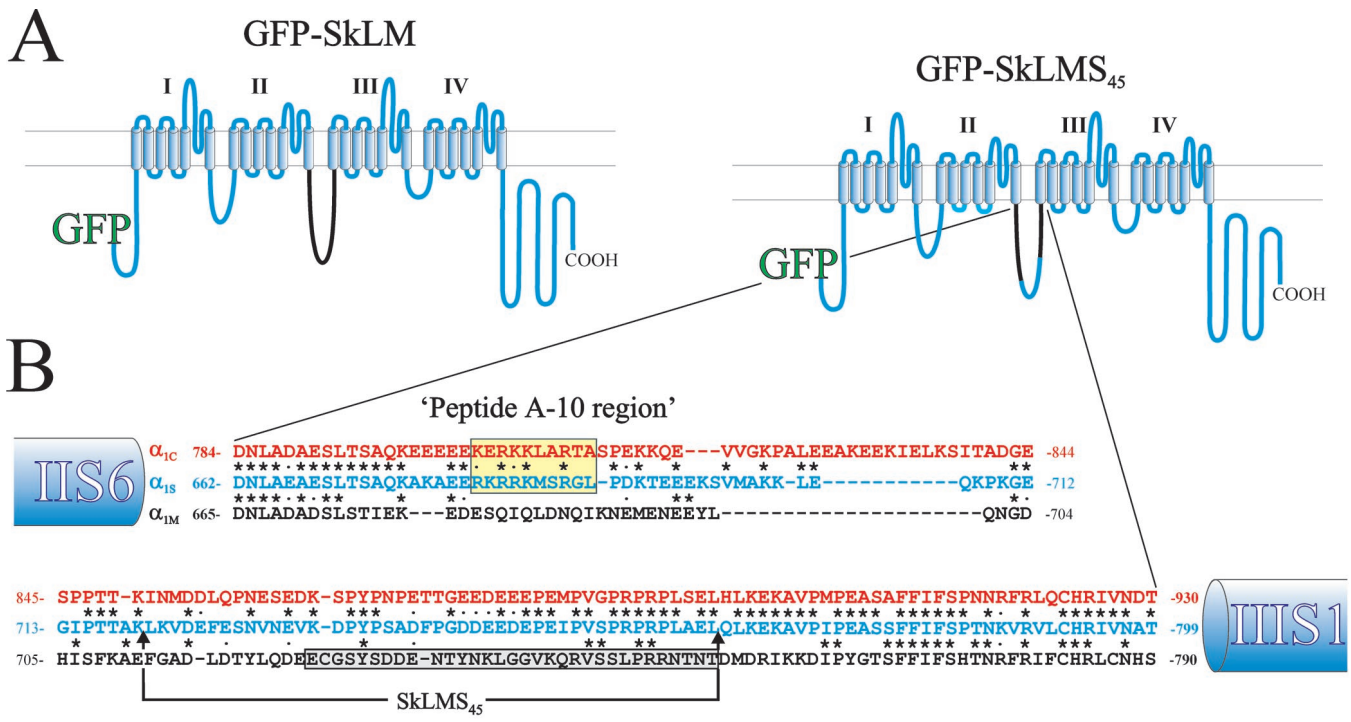

Fig. 1. Schematic representation of the skeletal/*Musca* II-III loop DHPR chimeras GFP-SkLM and GFP-SkLMS$_{45}$ and II-III loop sequence alignments. (*A*) DHPR chimeras were N-terminally fused to the green fluorescent protein GFP (19). Rabbit skeletal muscle (α_{1S}) sequence is indicated in blue, and *M. domestica* (house fly) muscle (α_{1M}) sequence is in black. I-IV, four homologous repeats of α_1 subunits. (*B*) Alignment of cardiac (α_{1C}), skeletal (α_{1S}), and *Musca* (α_{1M}) II-III loop sequences. The *Musca* sequence boxed in light gray (α_{1M} residues E724–T755) was replaced by the portion of α_{1S} sequence indicated by arrows (residues L720–L764) to yield GFP-SkLMS$_{45}$. Sequences boxed in yellow indicate the so-called skeletal and cardiac ''peptide A-10 region'' or ''activating domain'' of EC coupling (12, 15). Asterisks indicate amino acids identical between α_{1S} and α_{1C} or α_{1S} and α_{1M}. Dots show corresponding residues with identical charge.

because the isolated peptide activates RyR1 (11–15). To test the role of the critical domain, we created the chimera GFP-SkLMS$_{45}$ (Fig. 1*A*), in which 32 residues (E724–T755) from the *Musca* loop of GFP-SkLM were replaced by α_{1S} residues L720–L764. In the absence of sequence homology that could serve as a guidepost for the insertion of the α_{1S} critical domain into the *Musca* II-III loop, we chose to make this insertion within GFP-SkLMS$_{45}$, such that the critical domain was separated from IIS6 and from IIIS1 by the same number of residues as in wild-type α_{1S}. The final residue (Q765) of α_{1S} sequence tested previously in α_{1S}/α_{1C} chimeras (8, 9) was omitted for cloning reasons.

The Presence of α_{1S} Residues 720–764 in the *Musca* II-III Loop Supports Retrograde Coupling. Expression of GFP-SkLM in dysgenic myotubes resulted in the presence of slowly activating (skeletal-type) Ca^{2+} currents, but these currents were much smaller than those for GFP-α_{1S} (Fig. 2*A*). To determine whether a reduced density of surface expression could account for the small Ca^{2+} currents produced by SkLM, we measured immobilization-resistant charge movements (Fig. 2*B*). The charge vs. voltage relationship then was fitted to determine the maximal charge movement (Q_{max}) as an indirect measure of the expression density of DHPRs in the plasma membrane. Additionally, the current–voltage relationship for each cell was fitted (24) to yield a value of maximal Ca^{2+} conductance (G_{max}). For each of the constructs, GFP-α_{1S} and GFP-SkLM, neither G_{max} nor Q_{max} was found to differ significantly between injected primary dysgenic myotubes and transfected GLT myotubes (Table 1). Thus, data from the two types of dysgenic myotubes were combined for all subsequent analyses. As shown in Fig. 2*C*, the average G_{max} was significantly smaller for GFP-SkLM than for GFP-α_{1S}, whereas Q_{max} was similar for the two constructs. Because the Q_{max} values are similar, it appears that the *Musca* loop does not alter surface expression and that the reduction in current amplitude occurs because the *Musca* loop does not support retrograde signaling with the RyR1. Unlike GFP-SkLM, GFP-SkLMS$_{45}$ produced Ca^{2+} currents (Fig. 2*A*) similar in magnitude to those of GFP-α_{1S}. This similarity between GFP-SkLMS$_{45}$ and GFP-α_{1S} also was evident in the average values of G_{max} (Fig. 2*C*). Thus, the presence in the II-III loop of α_{1S} residues L720–L764, even when surrounded by sequence very unlike α_{1S}, was sufficient to restore the retrograde interaction whereby RyR1 increases the magnitude of slow L type Ca^{2+} current.

The Presence of α_{1S} Residues 720–764 in the *Musca* II-III Loop Supports Orthograde Coupling. In GLT myotubes expressing GFP-α_{1S}, brief depolarizing pulses elicited transient elevations of intracellular Ca^{2+}, which persisted even when Ca^{2+} influx was blocked by the addition of Cd^{2+} and La^{3+} to the bath (Fig. 3*A*). By contrast, the addition of Cd^{2+} and La^{3+} abolished the depolarization-evoked Ca^{2+} transients in GLT myotubes expressing GFP-α_{1C}, although the SR was still capable of releasing Ca^{2+} in response to caffeine (Fig. 3*B*). Thus, GLT myotubes provide an appropriate system for distinguishing skeletal-type transients, which do not depend on entry of extracellular Ca^{2+}, from cardiac-type transients, which do depend on such Ca^{2+} entry. Brief depolarizations failed entirely to evoke transients in GLT myotubes expressing GFP-SkLM, although the response to caffeine indicated that SR Ca^{2+} release was functional in these cells (Fig. 3*C*). By contrast, skeletal-type transients were present in GLT myotubes expressing GFP-SkLMS$_{45}$ (Fig. 3*D*). As a more quantitative measurement of the strength of EC coupling, we determined for each chimeric construct the fraction of injected primary myotubes that contracted in response to electrical stimulation in Cd^{2+}/La^{3+} solution. Contractions were never observed for GFP-

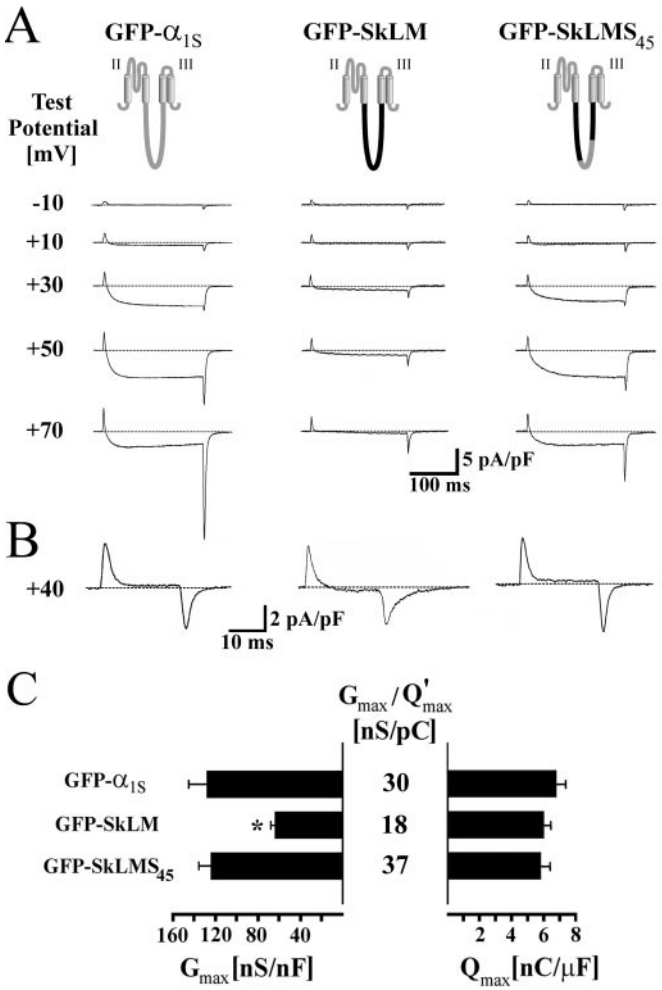

Fig. 2. Restoration of retrograde coupling after insertion of α_{1S} residues 720–764 into the *Musca* II-III loop (chimera GFP-SkLMS$_{45}$). (*A*) Representative whole-cell Ca^{2+} currents recorded from dysgenic myotubes expressing GFP-α_{1S} (*Left*), GFP-SkLM (*Center*), and GFP-SkLMS$_{45}$ (*Right*). After a prepulse to inactivate T type currents (24), macroscopic Ca^{2+} currents were elicited by 200-ms step depolarizations from a holding potential of −80 mV to the indicated test potentials. Current amplitudes were normalized by linear cell capacitance and are expressed as pA/pF. (*B*) Representative immobilization-resistant intramembrane charge movements measured at +40 mV after blocking Ca^{2+} currents with 0.5 mM Cd^{2+} and 0.1 mM La^{3+}, recorded from cells expressing the same three constructs shown above. (*C*) Average maximal Ca^{2+} conductance (G_{max}, *Left*) and charge movement (Q_{max}, *Right*) and ratios of G_{max}/Q'_{max} (*Center*) for GFP-α_{1S}, GFP-SkLM, and GFP-SkLMS$_{45}$. The asterisk indicates a statistically significant ($P < 0.001$) difference in average G_{max} from the other two constructs after comparison by an unpaired two-sample *t* test. No asterisk indicates lack of statistically significant difference ($P > 0.05$). (Bars = mean ± SEM of 12–20 recordings.)

SkLM, whereas the fraction of contracting myotubes was comparable for GFP-SkLMS$_{45}$ and GFP-α_{1S} (Fig. 3*E*). Like myotubes from normal mice (data not shown), electrical stimulation failed to cause contraction of a fraction of dysgenic myotubes transfected with GFP-α_{1S} or GFP-SkLMS$_{45}$. These noncontracting cells most likely represent myotubes in which components of the excitation–contraction coupling machinery are not fully developed (see ref. 25).

In addition to examining EC coupling in intact myotubes, we also used whole-cell patch clamping to characterize the voltage dependence of Ca^{2+} release in primary dysgenic myotubes expressing GFP-α_{1S}, GFP-SkLM, and GFP-SkLMS$_{45}$. Very small Ca^{2+} transients were present for GFP-SkLM (Fig. 4*A*). Moreover, these transients appeared to depend on Ca^{2+} entry because the amplitude of the transient had a voltage dependence

Table 1. Ca^{2+} conductance and charge movement properties recorded from primary dysgenic myotubes and from the dysgenic cell line GLT are highly comparable

Construct	G_{max}, nS/nF	Q_{max}, nC/μF	G_{max}/Q'_{max}, nS/pC
GFP-α_{1S}	*154 ± 16 (15)*	*7.5 ± 0.8 (15)*	*31*
	127 ± 16 (13)	6.8 ± 0.5 (13)	30
GFP-SkLM	*60 ± 5 (14)*	*6.1 ± 0.4 (14)*	*17*
	67 ± 15 (6)	6.0 ± 1.4 (6)	19

Data are given as mean ± SEM (numbers in parentheses are the myotubes tested). Recordings from primary dysgenic myotubes (cDNA injected) are indicated in *italic* and from immortalized dysgenic GLT myotubes (cDNA transfected) in roman. G_{max} is the maximal Ca^{2+} conductance (currents fitted according to ref. 24), Q_{max} is the maximum immobilization-resistant charge movement (Q_{on} fitted according to ref. 24), and Q'_{max} is the difference between Q_{max} and the average, endogenous charge movement $Q_{dys(max)}$ found in dysgenic myotubes ($Q_{dys(max)}$ = 2.5 nC/μF; ref. 24). Brackets indicate a lack of significant difference ($P > 0.05$) between data sets compared by an unpaired two-sample *t* test. Values for GFP-α_{1S} recorded from primary dysgenic myotubes were listed for comparison and were published (9).

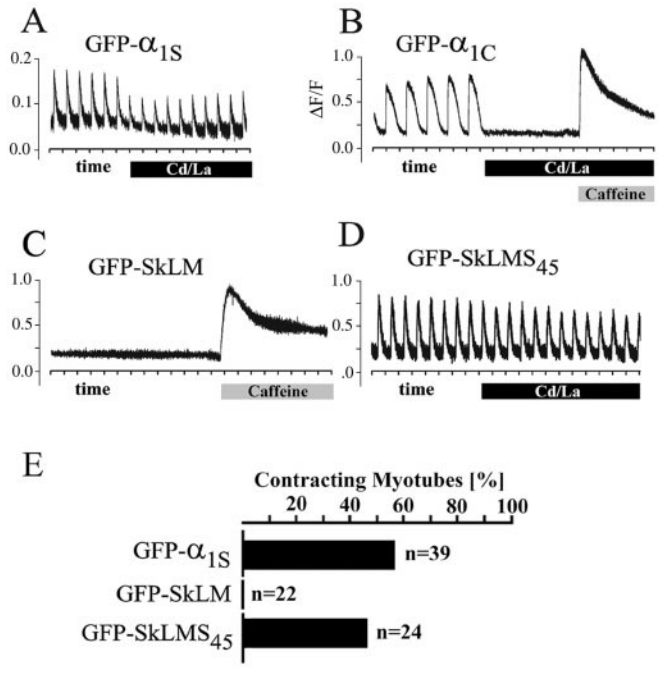

Fig. 3. Chimera GFP-SkLMS$_{45}$ restores skeletal-type EC coupling on expression in dysgenic myotubes. Action-potential-induced Ca^{2+} transients recorded from dysgenic myotubes expressing DHPR constructs, loaded with the fluorescent Ca^{2+} indicator Fluo-4 AM. Tick marks on the horizontal axes indicate 2 s. The skeletal GFP-α_{1S} (*A*) responded to 1-ms stimuli with Ca^{2+} transients that persisted after blocking currents with 0.5 mM Cd^{2+} and 0.1 mM La^{3+} (solid bar), whereas the cardiac GFP-α_{1C} Ca^{2+} transients (*B*) were blocked by the Cd^{2+}/La^{3+} solution. Myotubes expressing GFP-SkLM (*C*) failed to restore action-potential-induced Ca^{2+} transients (n = 10 dishes) even though Ca^{2+} release could be induced with 6 mM caffeine (shaded bar). GFP-SkLMS$_{45}$ (*D*) fully restored action-potential-induced Ca^{2+} transients that were resistant to Cd^{2+}/La^{3+} block of Ca^{2+} currents, indicating skeletal-type EC coupling. As for GFP-α_{1S}, the application of Cd^{2+}/La^{3+} sometimes caused a modest reduction in the amplitude of the transient in cells expressing GFP-SkLMS$_{45}$. (*E*) Electrically evoked contractions (100 ms, 100 V) recorded in Cd^{2+}/La^{3+} from dysgenic myotubes expressing either GFP-α_{1S}, GFP-SkLM, or GFP-SkLMS$_{45}$ indicated as percentage of myotubes stimulated.

PHYSIOLOGY

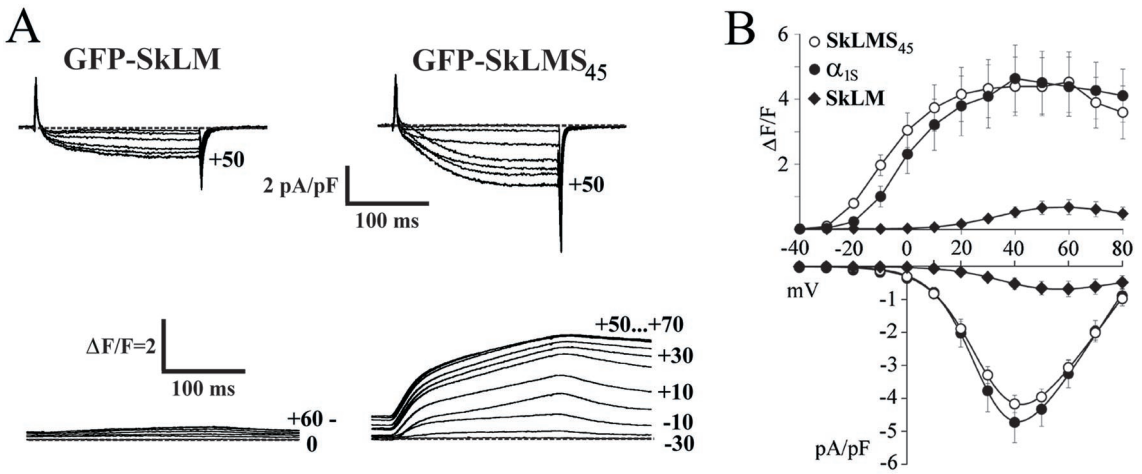

Fig. 4. Restoration of bidirectional coupling by expression of chimera GFP-SkLMS$_{45}$. (*A*) Whole-cell Ca^{2+} currents (*Upper*) and depolarization-induced Ca^{2+} transients (*Lower*) recorded simultaneously from dysgenic myotubes expressing GFP-SkLM or GFP-SkLMS$_{45}$. Step depolarizations (200-ms pulses) were applied in 10-mV increments from a holding potential of −80 mV after a prepulse protocol (24). The vertical scale indicates ΔF/F, Ca^{2+}-induced Fluo-3 fluorescence increments (ΔF) with respect to basal fluorescence (F). (*B*) Voltage dependence of depolarization-induced Ca^{2+} transients (ΔF/F, *Upper*) and of peak current densities (pA/pF, *Lower*) recorded from dysgenic myotubes expressing GFP-α_{1S} (●), GFP-SkLM (◆), and GFP-SkLMS$_{45}$ (○). Values represent the mean ± SEM of 11–20 recordings. The small Ca^{2+} transients for GFP-SkLM appeared to be a direct consequence of Ca^{2+} influx through the DHPR (see text).

mirroring that of Ca^{2+} current (Fig. 4*B*). Additionally, the Ca^{2+} transients for GFP-SkLM were blocked by the addition of Cd^{2+} and La^{3+} to the bath (data not shown). In myotubes expressing GFP-SkLMS$_{45}$, the Ca^{2+} transients were large (Fig. 4*A*) and did not differ significantly in either magnitude or voltage dependence from those of GFP-α_{1S} (Fig. 4*B*). Thus, placing α_{1S} residues L720–L764 into the very dissimilar background of the *Musca* II-III loop was able to restore both orthograde and retrograde coupling with RyR1.

A prerequisite for the bidirectional interaction between a DHPR construct and RyR1 is the colocalization of the two proteins in junctions between the plasma membrane and SR. If GFP-SkLM were not targeted into junctions, this could explain the absence of bidirectional signaling observed for this construct. Fig. 5 compares the subcellular distribution of GFP-SkLM (*Top*) with that of RyR1 (*Middle*). Both proteins are present in discrete clusters that overlap with one another, and clusters were observed in 54% of transfected myotubes ($n = 200$), which is close to the value observed in GFP-α_{1S}-transfected myotubes (58%; $n = 967$). This colocalization, which indicates correct junctional targeting, is particularly evident in the pseudocolor overlay image (Fig. 5 *Bottom*), in which green and red indicate GFP-SkLM and RyR1, respectively, and yellow shows sites of colocalization. Because GFP-SkLM is able to target to junctions between the plasma membrane and SR, and because its targeting is not different from that of GFP-SkLMS$_{45}$ [clusters found in 58% of transfected myotubes ($n = 65$); micrograph not shown], a failure to colocalize cannot account for the lack of bidirectional signaling by GFP-SkLM.

EC coupling in skeletal muscle likely involves allosteric coupling between α_{1S} and RyR1 either by direct contact between the two proteins or by way of intervening proteins. Using chimeras based on the II-III loop of the *Musca* DHPR, we have shown that residues L720–L764 of α_{1S} contain a critical domain that is essential for both EC coupling and retrograde signaling. This result is in agreement with previous work using chimeras based on the II-III loop of α_{1C} (8, 9). The new finding that bidirectional signaling survives a drastic change in the sequence of the As10 region makes it very unlikely that this region plays an important role in the activation of RyR1 during EC coupling as postulated previously (12, 13, 16). A similar conclusion also was reached on

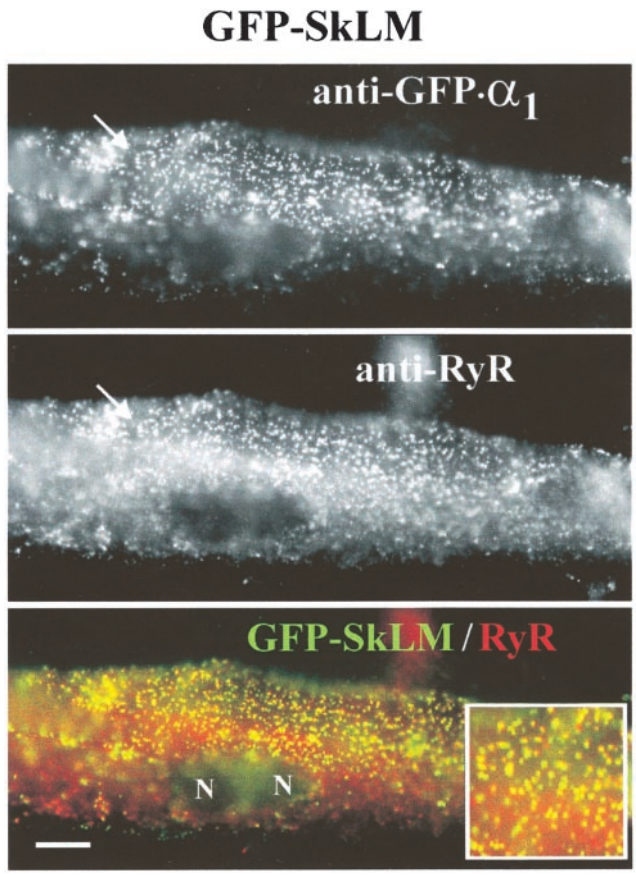

Fig. 5. Reduced Ca^{2+} currents and lack of EC coupling are not a result of failed junctional targeting of chimera GFP-SkLM. Subcellular localization of chimera GFP-SkLM in a transiently transfected dysgenic myotube (GLT). Double-immunofluorescence labeling was performed with antibodies against GFP, N-terminally fused to the DHPR chimera (*Top*) and against RyR1 (*Middle*). The ''merged image'' (*Bottom*) emphasizes the colocalization (yellow foci) of GFP-SkLM (green) and RyR1 (red) in clusters that represent junctions of the SR with transverse tubules or with the plasma membrane. Arrows indicate examples of GFP-SkLM/RyR1 colocalization. *Inset* shows a 2-fold-enlarged view of coclustered channels. N, nuclei. (Bar = 10 μm.)

the basis of a skeletal DHPR in which only the As10 region was scrambled (30).

A model of allosteric coupling between α_{1S} and RyR1 would appear to have two requirements. First, there must be anchoring interactions that maintain α_{1S} and RyR1 in a precise spatial coordination with respect to one another. Second, the allosteric coupling between α_{1S} and RyR1 during orthograde signaling must involve one or more cytoplasmic domains of α_{1S} that undergo conformational changes in response to movement of the voltage-sensing domains. Thus, the critical domain of the II-III loop could be involved in protein–protein interactions that were either static (anchoring) or dynamic (undergoing conformational changes during orthograde signaling) or both. If the critical domain plays a dynamic role in EC coupling, then conformational changes are unlikely to be transmitted to it via the peptide backbone because signaling is normal after large changes in the sequence of the flanking regions. Whatever the role of the critical domain, the important result of the present work is that bidirectional signaling is *not* affected by dramatic changes in the primary sequence of the loop regions that flank the critical domain. Thus, these flanking regions are unlikely to be sites of protein–protein interaction necessary for bidirectional signaling.

We thank L. Grimes, K. Parsons, E. Emberger, and Dr. J. Hoflacher for their excellent experimental help and Dr. H. Glossmann for continuous support. This work was supported in part by Grants P13831-GEN (to M.G.) and P12653-MED (to B.E.F.) from the Fonds zur Förderung der wissenschaftlichen Forschung, Austria, by European Commissions Training and Mobility of Researchers Network Grant ERBFMRXCT960032 (to B.E.F.), and by National Institutes of Health Grant NS 24444 (to K.G.B.).

1. Flucher, B. E. & Franzini-Armstrong, C. (1996) *Proc. Natl. Acad. Sci. USA* **93,** 8101–8106.
2. Franzini-Armstrong, C. & Protasi, F. (1997) *Physiol. Rev.* **77,** 699–729.
3. Schneider, M. F. & Chandler, W. K. (1973) *Nature (London)* **242,** 244–246.
4. Rios, E. & Brum, G. (1987) *Nature (London)* **325,** 717–720.
5. Nakai, J., Dirksen, R. T., Nguyen, H. T., Pessah, I. N., Beam, K. G. & Allen, P. D. (1996) *Nature (London)* **380,** 72–75.
6. Chaudhari, N. (1992) *J. Biol. Chem.* **267,** 25636–25639.
7. Tanabe, T., Beam, K. G., Adams, B. A., Niidome, T. & Numa, S. (1990) *Nature (London)* **346,** 567–569.
8. Nakai, J., Tanabe, T., Konno, T., Adams, B. & Beam, K. G. (1998) *J. Biol. Chem.* **273,** 24983–24986.
9. Grabner, M., Dirksen, R. T., Suda, N. & Beam, K. G. (1999) *J. Biol. Chem.* **274,** 21913–21922.
10. Lu, X., Xu, L. & Meissner, G. (1994) *J. Biol. Chem.* **269,** 6511–6516.
11. El-Hayek, R., Antoniu, B., Wang, J., Hamilton, S. L. & Ikemoto, N. (1995) *J. Biol. Chem.* **270,** 22116–22118.
12. El-Hayek, R. & Ikemoto, N. (1998) *Biochemistry* **37,** 7015–7020.
13. Dulhunty, A. F., Laver, D. R., Gallant, E. M., Casarotto, M. G., Pace, S. M. & Curtis, S. (1999) *Biophys. J.* **77,** 189–203.
14. Casarotto, M. G., Gibson, F., Pace, S. M., Curtis, S. M., Mulcair, M. & Dulhunty, A. F. (2000) *J. Biol. Chem.* **275,** 11631–11637.
15. Saiki, Y., El-Hayek, R. & Ikemoto, N. (1999) *J. Biol. Chem.* **274,** 7825–7832.
16. Zhu, X., Gurrola, G., Jiang, M. T., Walker, J. W. & Valdivia, H. H. (1999) *FEBS Lett.* **450,** 221–226.
17. Grabner, M., Bachmann, A., Rosenthal, F., Striessnig, J., Schultz, C., Tautz, D. & Glossmann, H. (1994) *FEBS Lett.* **339,** 189–194.
18. Tanabe, T., Takeshima, H., Mikami, A., Flockerzi, V., Takahashi, H., Kangawa, K., Kojima, M., Matsuo, H., Hirose, T. & Numa, S. (1987) *Nature (London)* **328,** 313–318.
19. Grabner, M., Dirksen, R. T. & Beam, K. G. (1998) *Proc. Natl. Acad. Sci. USA* **95,** 1903–1908.
20. Adams, B. A. & Beam, K. G. (1989) *J. Gen. Physiol.* **94,** 429–444.
21. Powell, J. A., Petherbridge, L. & Flucher, B. E. (1996) *J. Cell Biol.* **134,** 375–387.
22. Tanabe, T., Beam, K. G., Powell, J. A. & Numa, S. (1988) *Nature (London)* **336,** 134–139.
23. Hamill, O. P., Marty, A., Neher, E., Sakmann, B. & Sigworth, F. J. (1981) *Pflügers Arch.* **391,** 85–100.
24. Adams, B. A., Tanabe, T., Mikami, A., Numa, S. & Beam, K. G. (1990) *Nature (London)* **346,** 569–572.
25. Flucher, B. E., Kasielke, N. & Grabner, M. (2000) *J. Cell Biol.* **151,** 467–477.
26. Garcia, J. & Beam, K. G. (1994) *J. Gen. Physiol.* **103,** 107–123.
27. Flucher, B. E., Andrews, S. B. & Daniels, M. P. (1994) *Mol. Biol. Cell.* **5,** 1105–1118.
28. Giannini, G., Conti, A., Mammarella, S., Scrobogna, M. & Sorrentino, V. (1995) *J. Cell Biol.* **128,** 893–904.
29. Sinnegger, M. J., Wang, Z., Grabner, M., Hering, S., Striessnig, J., Glossmann, H. & Mitterdorfer, J. (1997) *J. Biol. Chem.* **272,** 27686–27693.
30. Proenza, C., Wilkens, C. M. & Beam, K. G. (2000) *J. Biol. Chem.* **275,** 29935–29937.